

(continued from page 379)

finite-difference solutions, and will describe one of the most straightforward (and student-friendly) finite-difference methods, namely MacCormack's technique. We will mention the idea of stability criteria—what is necessary to ensure stable numerical calculations. The two philosophies for dealing with shock waves in these numerical solutions—shock capturing and shock fitting—will be discussed. Finally, we end the chapter with an illustration of the application of both the

method of characteristics and the finite-difference technique to the calculation of the flow over the Space Shuttle.

*Note:* For a very introductory presentation of computational fluid dynamics, see Anderson, *Computational Fluid Dynamics: The Basics with Applications*, McGraw-Hill, 1995. This book is written to be used before you study any of the other, more advanced books on CFD.

## 11.1 | AN INTRODUCTION TO COMPUTATIONAL FLUID DYNAMICS

As we have seen from the previous chapters, the cornerstone of theoretical fluid dynamics is a set of conservation equations that describe the physics of fluid motion; these equations speak words, such as: (1) mass is conserved; (2)  $\mathbf{F} = m\mathbf{a}$  (Newton's second law); and (3) energy is conserved. These equations also describe the variations of fluid pressure, temperature, density, velocity, etc., throughout space and time. In their most general form, they are integral equations (see Chap. 2) or partial differential equations (see Chap. 6), and consequently are difficult to solve. Indeed, no general analytical solution to these equations has been found, nor is it likely to be found in the foreseeable future. For the two centuries since Bernoulli and Euler first formulated some of these equations in St. Petersburg, Russia, in the 1730s, fluid dynamicists have been laboring to obtain analytical solutions for certain restricted and/or simplified problems. The preceding chapters of this book have dealt primarily with such (relatively speaking) simplified problems.

In contrast, the modern engineer of today is operating in a new third dimension in fluid dynamics—*computational fluid dynamics*, which readily complements the previous dimensions of pure experiment and pure theory. Computational fluid dynamics, in principle, allows the practical solution of the exact governing equations for a myriad of applied engineering problems, and it is this aspect that is introduced in this chapter and carried through all the remaining chapters of this book.

What is computational fluid dynamics? It is the art of replacing the individual terms in the governing conservation equations with discretized algebraic forms, which in turn are solved to obtain *numbers* for the flowfield variables at discrete points in time and/or space. The end product of CFD is indeed a collection of numbers, in contrast to a closed-form analytical solution. However, in the long run, the objective of most engineering analyses, closed form or otherwise, is a quantitative description of the problem, i.e., *numbers*. If the governing conservation equations are given in integral form, the integral terms themselves are replaced with discrete algebraic expressions involving the flowfield variables at discrete grid points distributed throughout the flow. This is called the *finite-volume technique*. If the equations are

given in partial differential equation form, the partial derivative terms are replaced with discrete algebraic difference quotients involving the flowfield variables at discrete grid points. This is called the *finite-difference technique*. In this book, our utilization of CFD will involve the finite-difference technique.

Perhaps the first major example of computational fluid dynamics applied to a practical engineering problem was the work of Kopal (Ref. 28), who in 1947 compiled massive tables of the supersonic flow over sharp cones by numerically solving the governing Taylor-Maccoll differential equation [see Chap. 10, and specifically Eqs. (10.13) and (10.15)]. The solutions were carried out on a primitive digital computer at the Massachusetts Institute of Technology. However, the first major generation of computational fluid-dynamic solutions appeared during the 1950s and early 1960s, spurred by the simultaneous advent of efficient, high-speed computers and the need to solve the high-velocity, high-temperature reentry body problem. High temperatures necessitated the inclusion of molecular vibrational energies and chemical reactions in flow problems, sometimes in equilibrium and at other times in non-equilibrium. As we shall see in Chaps. 16 and 17, such high-temperature physical phenomena generally cannot be solved analytically, even for the simplest flow geometry. Therefore, numerical solutions of the governing equations on a high-speed computer were an absolute necessity. Even though it was not fashionable at the time to describe such high-temperature gasdynamic calculations as “computational fluid dynamics,” they nevertheless represented the first generation of the discipline.

The second generation of computational fluid-dynamic solutions, those that today are generally descriptive of the discipline, involve the application of the general equations of motion to applied fluid-dynamic problems that are in themselves so complicated (without the presence of chemical reactions, etc.) that a computer must be utilized. Examples of such inherently difficult problems are mixed subsonic-supersonic flows such as the supersonic blunt body problem (to be discussed in Chap. 12), and viscous flows which are not amenable to the boundary layer approximation, such as separated and recirculating flows. In the latter case, the full Navier-Stokes equations are required for an exact solution. Such viscous flows are outside the scope of this book; here we will deal with inviscid flows only.

Two major numerical techniques for the solution of completely supersonic, steady inviscid flows are introduced in this chapter—the method of characteristics and finite-difference methods. The method of characteristics is older and more developed, and is limited to inviscid flows, whereas finite-difference techniques (along with finite-volume techniques) are still evolving as computational fluid dynamics grows and matures, and have much more general application to inviscid and viscous flows. In this chapter, only some flavor and general guidance on finite-difference solutions can be given. Computational fluid dynamics is an extensive subject on its own, and its detailed study is beyond the scope of this book. Some early surveys of CFD can be found in Refs. 30 through 33. Some excellent modern textbooks on CFD at the graduate level are now available; see for examples Refs. 102 and 137 through 142. For a text written specifically for an elementary introduction to CFD, intended to be read before studying some of the more advanced texts, see Ref. 18. The reader is strongly encouraged to examine this literature in order to develop a more substantial

understanding of CFD. In addition to the introduction given in the present chapter, all the remaining chapters of this book deal to a greater or lesser extent with computational techniques. However, in all cases our discussions will be self-contained; you are not expected to be familiar with the details of CFD. Indeed, the main thrust of this book is to emphasize the *physical* fundamentals of compressible flow, not to constitute a study of detailed mathematical or computational methods. But if this material whets your appetite to look further into CFD, you now know where to look.

Finally, the numerical techniques discussed in the remainder of this chapter have three aspects in common:

1. They involve the calculation of flowfield properties at discrete points in the flow. For example, consider an  $xy$  coordinate space that is divided into a rectangular grid, as sketched in Fig. 11.3. The solid circles denote *grid points* at which the flow properties are either known or to be calculated. The points are indexed by the letters  $i$  in the  $x$  direction and  $j$  in the  $y$  direction. For example, the point directly in the middle of the grid is denoted by  $(i, j)$ , the point immediately to its right is  $(i + 1, j)$ , and so forth. It is not necessary to always deal with a rectangular grid as shown in Fig. 11.3, although such grids are preferable for finite-difference solutions. For the method of characteristics solutions, we will deal with a nonrectangular grid.
2. They are predicated on the ability to expand the flowfield properties in terms of a Taylor's series. For example, if  $u_{i,j}$  denotes the  $x$  component of velocity known at point  $(i, j)$ , then the velocity  $u_{i+1,j}$  at point  $(i + 1, j)$  can be obtained from

$$u_{i+1,j} = u_{i,j} + \left( \frac{\partial u}{\partial x} \right)_{i,j} \Delta x + \left( \frac{\partial^2 u}{\partial x^2} \right)_{i,j} \frac{(\Delta x)^2}{2} + \dots \quad (11.1)$$

Equation (11.1) will be useful in the subsequent sections.

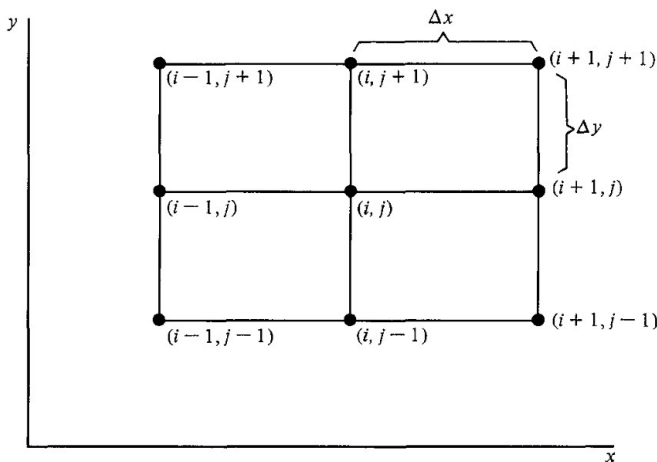


**Figure 11.3** | Rectangular finite-difference grid.

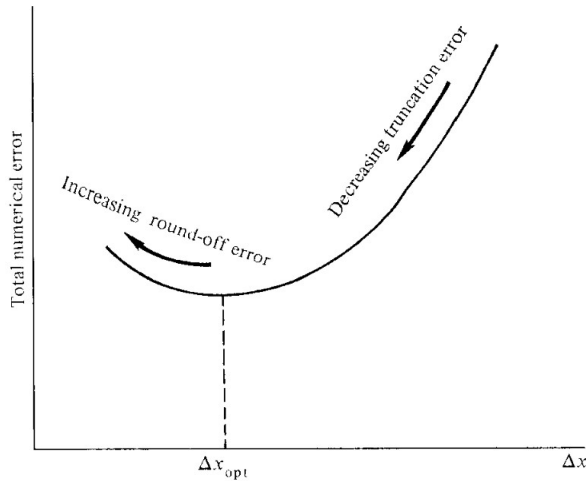


**Figure 11.4** | Schematic of the effect of grid size on numerical error.

3. In the theoretical limit of an infinite number of grid points (i.e.,  $\Delta x$  and  $\Delta y \rightarrow 0$  in Fig. 11.3), the solutions are *exact*. Since all practical calculations obviously utilize a finite number of grid points, such numerical solutions are subject to *truncation error*, due to neglect of the higher-order terms in Eq. (11.1). Moreover, because all digital computers round off each number to a certain significant figure, the flowfield calculations are also subject to *round-off error*. By reducing the value of  $\Delta x$  in Eq. (11.1), the truncation error is reduced; however, the number of steps required to calculate a certain distance in  $x$  is correspondingly increased, therefore increasing the round-off error. This trend is illustrated in Fig. 11.4, which shows the total numerical error as a function of step size,  $\Delta x$ . Note that there is an optimum value  $(\Delta x)_{\text{opt}}$  at which maximum accuracy is obtained; it does *not* correspond to  $\Delta x \rightarrow 0$ . Although all computations are subject to these numerical errors, this author feels that, as long as the full nonlinear equations of motion are being solved along with the exact boundary conditions, such solutions are properly designated as *exact solutions*. Therefore, an important advantage of computational fluid dynamics is its inherent ability to provide exact solutions to difficult, nonlinear problems.

## 11.2 | PHILOSOPHY OF THE METHOD OF CHARACTERISTICS

Let us begin to obtain a feeling for the method of characteristics by considering again Fig. 11.3 and Eq. (11.1). Neglect the second-order term in Eq. (11.1), and write

$$u_{i+1,j} = u_{i,j} + \left( \frac{\partial u}{\partial x} \right)_{i,j} \Delta x + \dots \quad (11.2)$$

The value of the derivative  $\partial u / \partial x$  can be obtained from the general conservation equations. For example, consider a two-dimensional irrotational flow, so that Eq. (8.17) yields, in terms of velocities,

$$\left(1 - \frac{u^2}{a^2}\right) \frac{\partial u}{\partial x} + \left(1 - \frac{v^2}{a^2}\right) \frac{\partial v}{\partial y} - \frac{2uv}{a^2} \frac{\partial u}{\partial y} = 0 \quad (11.3)$$

Solve Eq. (11.3) for  $\partial u / \partial x$ :

$$\frac{\partial u}{\partial x} = \frac{\frac{2uv}{a^2} \frac{\partial u}{\partial y} - \left(1 - \frac{v^2}{a^2}\right) \frac{\partial v}{\partial y}}{(1 - u^2/a^2)} \quad (11.4)$$

Now assume the velocity  $\mathbf{V}$ , and hence  $u$  and  $v$ , is known at each point along a vertical line,  $x = x_o$ , as sketched in Fig. 11.5. Specifically, the values of  $u$  and  $v$  are known at point  $(i, j)$ , as well as above and below, at points  $(i, j+1)$  and  $(i, j-1)$ . Hence, the  $y$  derivatives,  $\partial u / \partial y$  and  $\partial v / \partial y$ , are known at point  $(i, j)$ . (They can be calculated from finite-difference quotients, to be discussed later.) Consequently, the right-hand side of Eq. (11.4) yields a number for  $(\partial u / \partial x)_{i,j}$ , which can be substituted into Eq. (11.2) to calculate  $u_{i+1,j}$ . However, *there is one notable exception*: If the denominator of Eq. (11.4) is zero, then  $\partial u / \partial x$  is at least indeterminate, and may even be discontinuous. The denominator is zero when  $u = a$ , i.e., when the component of flow velocity perpendicular to  $x = x_o$  is sonic, as shown in Fig. 11.5. Moreover, from the geometry of Fig. 11.5, the angle  $\mu$  is defined by  $\sin \mu = u/V = a/V = 1/M$ , i.e.,  $\mu$  is the *Mach angle*. The orientation of the  $x$  and  $y$  axes with respect to  $\mathbf{V}$  in Fig. 11.5 is arbitrary; the germane aspect of this discussion is that a line that makes a Mach angle with respect to the streamline direction at a point is also a

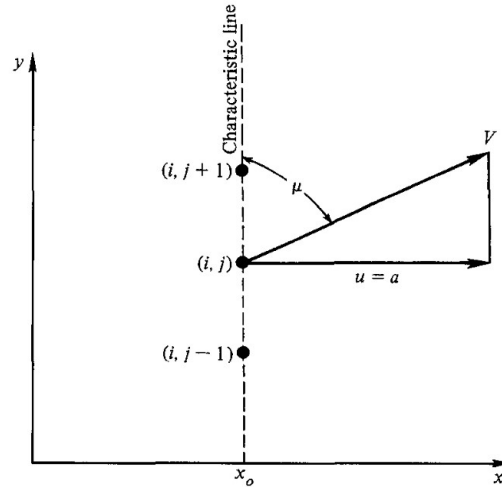


**Figure 11.5** | Illustration of the characteristic direction.

line along which the derivative of  $u$  is indeterminate, and across which it may be discontinuous. We have just demonstrated that such lines exist, and that they are Mach lines. The choice of  $u$  was arbitrary in the above discussion. The derivatives of the other flow variables,  $p$ ,  $\rho$ ,  $T$ ,  $v$ , etc., are also indeterminate along these lines. Such lines are defined as *characteristic lines*.

With this in mind, we can now outline the general philosophy of the method of characteristics. Consider a region of steady, supersonic flow in  $xy$  space. (For simplicity, we will initially deal with two-dimensional flow; extensions to three-dimensional flows will be discussed later.) This flowfield can be solved in three steps, as follows:

**Step 1.** Find some particular lines (directions) in the  $xy$  space where *flow variables* ( $p$ ,  $\rho$ ,  $T$ ,  $u$ ,  $v$ , etc.) are *continuous*, but along which the *derivatives* ( $\partial p/\partial x$ ,  $\partial u/\partial y$ , etc.) are *indeterminate*, and in fact across which the derivatives may even sometimes be discontinuous. As already defined, such lines in the  $xy$  space are called *characteristic lines*.

**Step 2.** Combine the partial differential conservation equations in such a fashion that ordinary differential equations are obtained that hold *only along the characteristic lines*. Such ordinary differential equations are called the *compatibility equations*.

**Step 3.** Solve the compatibility equations step by step *along* the characteristic lines, starting from the given initial conditions at some point or region in the flow. In this manner, the complete flowfield can be mapped out along the characteristics. In general, the characteristic lines (sometimes referred to as the “characteristics net”) depend on the flowfield, and the compatibility equations are a function of geometric location along the characteristic lines; hence, the characteristics and the compatibility equations must be constructed and solved simultaneously, step by step. An exception to this is two-dimensional irrotational flow, for which the compatibility equations become algebraic equations explicitly independent of geometric location. This will be made clear in subsequent sections.

As an analog to this discussion, the above philosophy is clearly exemplified in the unsteady, one-dimensional flow discussed in Chap. 7. Consider a centered expansion wave traveling to the left, as sketched in Fig. 11.6. In Chap. 7, the governing partial differential equations were reduced to ordinary differential equations (compatibility equations) which held only along certain lines in the  $xt$  plane that had slopes of  $dx/dt = u \pm a$ . The compatibility equations are Eqs. (7.65) and (7.66), and the lines were defined as characteristic lines in Sec. 7.6. These characteristics are sketched in Fig. 11.6a. However, in Chap. 7, we did not explicitly identify such characteristic lines with indeterminate or discontinuous derivatives. Nevertheless, this identification can be made by examining Eq. (7.89), which gives  $u = u(x, t)$ . Consider a given time  $t = t_1$ , which is illustrated by the dashed horizontal line in Fig. 11.6a. At time  $t_1$ , the head of the wave is located at  $x_b$ , and the tail at  $x_e$ . Equation (7.89) for the mass motion  $u$  is evaluated at time  $t_1$ , as sketched in Fig. 11.6b. Note that at  $x_b$  the velocity is continuous, but  $\partial u/\partial x$  is discontinuous across the leading characteristic. Similarly, at  $x_e$ ,  $u$  is continuous but  $\partial u/\partial x$  is discontinuous across

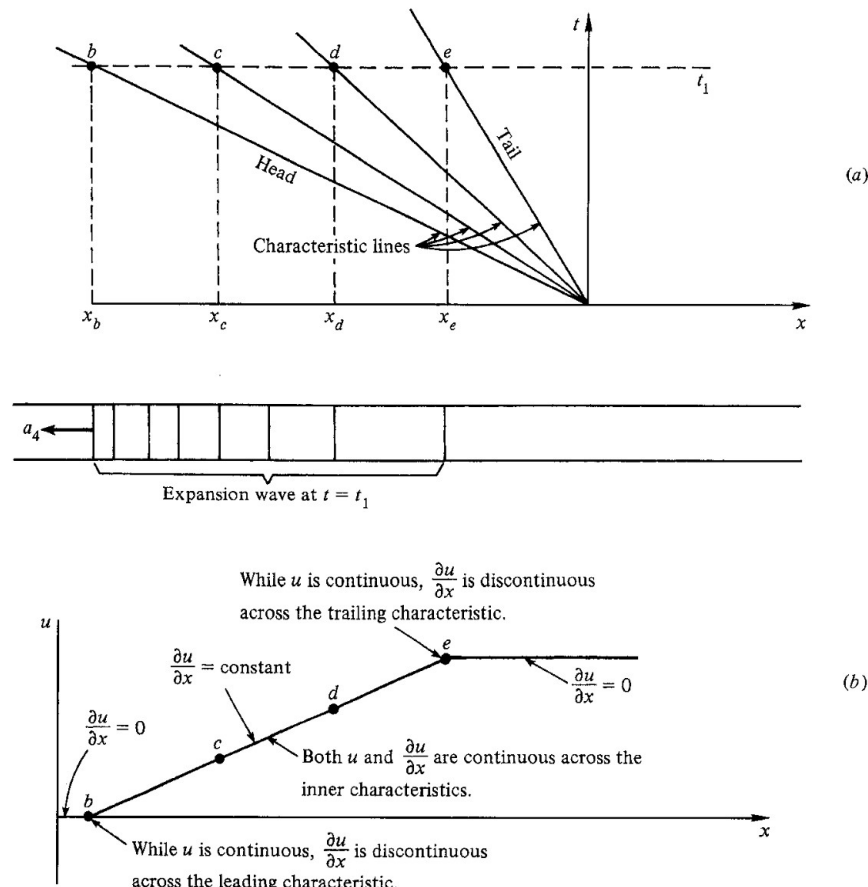


**Figure 11.6** | Relationship of characteristics in unsteady one-dimensional flow.

the trailing characteristic. Hence, by examining Fig. 11.6a and b, we see that the characteristic lines identified in Chap. 7 are indeed consistent with the definition of characteristics given in the present chapter.

### 11.3 | DETERMINATION OF THE CHARACTERISTIC LINES: TWO-DIMENSIONAL IRROTATIONAL FLOW

At the beginning of Sec. 11.2, Mach lines in the flow were identified as characteristic lines in a somewhat heuristic fashion. Are there other characteristic lines in the flow? Is there a more deterministic approach to identifying characteristic lines? Those questions are addressed in this section.

To begin with, consider steady, adiabatic, two-dimensional, irrotational supersonic flow. Other types of flow will be considered in subsequent sections. The governing nonlinear equations are Eqs. (8.17) and (8.18). For two-dimensional flow, Eq. (8.17) becomes

$$\left(1 - \frac{\Phi_x^2}{a^2}\right)\Phi_{xx} + \left(1 - \frac{\Phi_y^2}{a^2}\right)\Phi_{yy} - \frac{2\Phi_x\Phi_y}{a^2}\Phi_{xy} = 0 \quad (11.5)$$

Note that  $\Phi$  is the full-velocity potential, *not* the perturbation potential. In fact, in all of our work in this chapter, we are not using perturbations in any way. Hence,

$$\Phi_x = u \quad \Phi_y = v \quad \mathbf{V} = u\mathbf{i} + v\mathbf{j}$$

Recall that  $\Phi_x = f(x, y)$ ; hence,

$$d\Phi_x = \frac{\partial\Phi_x}{\partial x}dx + \frac{\partial\Phi_x}{\partial y}dy = \Phi_{xx}dx + \Phi_{xy}dy \quad (11.6)$$

$$d\Phi_y = \frac{\partial\Phi_y}{\partial x}dx + \frac{\partial\Phi_y}{\partial y}dy = \Phi_{xy}dx + \Phi_{yy}dy \quad (11.7)$$

Recopying these equations,

$$\text{From Eq. (11.5)} \quad \left(1 - \frac{u^2}{a^2}\right)\Phi_{xx} - \frac{2uv}{a^2}\Phi_{xy} + \left(1 - \frac{v^2}{a^2}\right)\Phi_{yy} = 0$$

$$\text{From Eq. (11.6)} \quad (dx)\Phi_{xx} + (dy)\Phi_{xy} = du$$

$$\text{From Eq. (11.7)} \quad (dx)\Phi_{xy} + (dy)\Phi_{yy} = dv$$

These equations can be treated as a system of simultaneous, linear, algebraic equations in the variables  $\Phi_{xx}$ ,  $\Phi_{yy}$ , and  $\Phi_{xy}$ . For example, using Cramer's rule, the solution for  $\Phi_{xy}$  is

$$\Phi_{xy} = \frac{\begin{vmatrix} 1 - \frac{u^2}{a^2} & 0 & 1 - \frac{v^2}{a^2} \\ dx & du & 0 \\ 0 & dv & dy \end{vmatrix}}{\begin{vmatrix} 1 - \frac{u^2}{a^2} & -\frac{2uv}{a^2} & 1 - \frac{v^2}{a^2} \\ dx & dy & 0 \\ 0 & dx & dy \end{vmatrix}} = \frac{N}{D} \quad (11.8)$$

Now consider point  $A$  and its surrounding neighborhood in an arbitrary flow-field, as sketched in Fig. 11.7. The derivative of the velocity potential,  $\Phi_{xy}$ , has a specific value at point  $A$ . Equation (11.8) gives the solution for  $\Phi_{xy}$  at point  $A$  for an arbitrary choice of  $dx$  and  $dy$ , i.e., for an arbitrary *direction* away from point  $A$  defined by the choice of  $dx$  and  $dy$ . For the chosen  $dx$  and  $dy$ , there are corresponding values of the change in velocity  $du$  and  $dv$ . No matter what values are chosen for  $dx$  and  $dy$ , the corresponding values of  $du$  and  $dv$  will always yield the same number for  $\Phi_{xy}$  from Eq. (11.8), *with one exception*. If  $dx$  and  $dy$  are chosen such that  $D = 0$

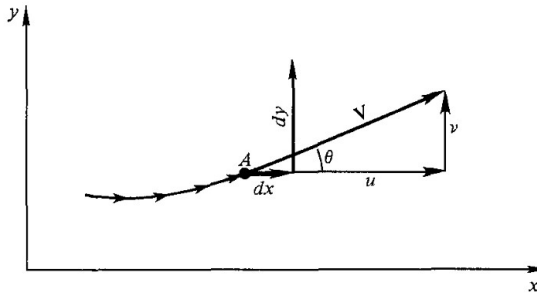


**Figure 11.7 | Streamline geometry.**

in Eq. (11.8), then  $\Phi_{xy}$  is not defined in that particular direction dictated by  $dx$  and  $dy$ . However, we know that  $\Phi_{xy}$  has a specific finite value at point  $A$ , even though it is not uniquely determined when the direction through point  $A$  is defined by this particular choice of  $dx$  and  $dy$ , which yields  $D = 0$  in Eq. (11.8). Clearly, an infinite value of  $\Phi_{xy}$  is physically inconsistent. For example, return to Fig. 11.6b. At points  $b$  and  $e$ ,  $\partial u/\partial x$  is not uniquely determined, but we have to say that its value should be somewhere between zero and the constant value given by the slope between points  $b$  and  $e$ . As a consequence, if the direction from  $A$  ( $dx$  and  $dy$ ) is chosen so that  $D = 0$  in Eq. (11.8), then to keep  $\Phi_{xy}$  finite,  $N = 0$  in Eq. (11.8) also:

$$\Phi_{xy} = \frac{N}{D} = \frac{0}{0}$$

That is,  $\Phi_{xy} = \partial u/\partial y = \partial v/\partial x$  is *indeterminate*. We have previously defined the directions in the flowfield along which the derivatives of the flow properties are indeterminate and across which they may be discontinuous as characteristic directions. Therefore, the lines in  $xy$  space for which  $D = 0$  (and hence  $N = 0$ ) are characteristic lines.

This now provides a means to calculate the equations of the characteristic lines. In Eq. (11.8) set  $D = 0$ . This yields

$$\left(1 - \frac{u^2}{a^2}\right)(dy)^2 + \frac{2uv}{a^2} dx dy + \left(1 - \frac{v^2}{a^2}\right)(dx)^2 = 0$$

or

$$\left(1 - \frac{u^2}{a^2}\right) \left(\frac{dy}{dx}\right)_{\text{char}}^2 + \frac{2uv}{a^2} \left(\frac{dy}{dx}\right)_{\text{char}} + \left(1 - \frac{v^2}{a^2}\right) = 0 \quad (11.9)$$

In Eq. (11.9),  $(dy/dx)_{\text{char}}$  is the slope of the characteristic lines. Using the quadratic formula, Eq. (11.9) yields

$$\left(\frac{dy}{dx}\right)_{\text{char}} = \frac{-2uv/a^2 \pm \sqrt{(2uv/a^2)^2 - 4[1 - (u^2/a^2)][1 - (v^2/a^2)]}}{2[1 - (u^2/a^2)]}$$

or

$$\left(\frac{dy}{dx}\right)_{\text{char}} = \boxed{\frac{-uv/a^2 \pm \sqrt{[(u^2 + v^2)/a^2] - 1}}{[1 - (u^2/a^2)]}} \quad (11.10)$$

Equation (11.10) defines the characteristic curves in the physical  $xy$  space.

Examine Eq. (11.10) more closely. The term inside the square root is

$$\frac{u^2 + v^2}{a^2} - 1 = \frac{V^2}{a^2} - 1 = M^2 - 1$$

Hence, we can state

1. If  $M > 1$ , there are two real characteristics through each point of the flowfield. Moreover, for this situation, Eq. (11.5) is defined as a *hyperbolic* partial differential equation.
2. If  $M = 1$ , there is one real characteristic through each point of the flow. By definition, Eq. (11.5) is a *parabolic* partial differential equation.
3. If  $M < 1$ , the characteristics are imaginary, and Eq. (11.5) is an *elliptic* partial differential equation.

Therefore, we see that steady, inviscid supersonic flow is governed by hyperbolic equations, sonic flow by parabolic equations, and subsonic flow by elliptic equations. Moreover, because two real characteristics exist through each point in a flow where  $M > 1$ , the method of characteristics becomes a practical technique for solving supersonic flows. In contrast, because the characteristics are imaginary for  $M < 1$ , the method of characteristics is not used for subsonic solutions. (An exception is transonic flow, involving mixed subsonic-supersonic regions, where solutions have been obtained in the complex plane using imaginary characteristics.) Also, it is worthwhile mentioning that the unsteady one-dimensional flow in Chap. 7 is hyperbolic, and hence two real characteristics exist through each point in the  $xt$  plane, as we have already seen. Indeed, *unsteady* inviscid flow is hyperbolic for two and three spatial dimensions, and for any speed regime—subsonic, transonic, supersonic, or hypersonic. This feature of unsteady flow underlies the strength of the time-dependent numerical technique to be described in Chap. 12.

Concentrating on steady, two-dimensional supersonic flow, let us examine the real characteristic lines given by Eq. (11.10). Consider a streamline as sketched in Fig. 11.7. At point  $A$ ,  $u = V \cos \theta$  and  $v = V \sin \theta$ . Hence, Eq. (11.10) becomes

$$\left( \frac{dy}{dx} \right)_{\text{char}} = \frac{\frac{-V^2 \cos \theta \sin \theta}{a^2} \pm \sqrt{\frac{V^2}{a^2} (\cos^2 \theta + \sin^2 \theta) - 1}}{1 - \frac{V^2}{a^2} \cos^2 \theta} \quad (11.11)$$

Recall that the Mach angle  $\mu$  is given by  $\mu = \sin^{-1}(1/M)$ , or  $\sin \mu = 1/M$ . Thus,  $V^2/a^2 = M^2 = 1/\sin^2 \mu$ , and Eq. (11.11) becomes

$$\left( \frac{dy}{dx} \right)_{\text{char}} = \frac{\frac{-\cos \theta \sin \theta}{\sin^2 \mu} \pm \sqrt{\frac{\cos^2 \theta + \sin^2 \theta}{\sin^2 \mu} - 1}}{1 - \frac{\cos^2 \theta}{\sin^2 \mu}} \quad (11.12)$$

From trigonometry,

$$\sqrt{\frac{\cos^2 \theta + \sin^2 \theta}{\sin^2 \mu} - 1} = \sqrt{\frac{1}{\sin^2 \mu} - 1} = \sqrt{\csc^2 \mu - 1} = \sqrt{\cot^2 \mu} = \frac{1}{\tan \mu}$$

Thus, Eq. (11.12) becomes

$$\left( \frac{dy}{dx} \right)_{\text{char}} = \frac{-\cos \theta \sin \theta / \sin^2 \mu \pm 1 / \tan \mu}{1 - (\cos^2 \theta / \sin^2 \mu)} \quad (11.13)$$

After more algebraic and trigonometric manipulation, Eq. (11.13) reduces to

$$\left( \frac{dy}{dx} \right)_{\text{char}} = \tan(\theta \mp \mu) \quad (11.14)$$

A graphical interpretation of Eq. (11.14) is given in Fig. 11.8, which is an elaboration of Fig. 11.7. At point A in Fig. 11.8, the streamline makes an angle  $\theta$  with the  $x$  axis. Equation (11.14) stipulates that there are two characteristics passing through point A, one at the angle  $\mu$  above the streamline, and the other at the angle  $\mu$  below the streamline. Hence, *the characteristic lines are Mach lines*. This fact was deduced in Sec. 11.2; however, the derivation given here is more rigorous. Also, the characteristic given by the angle  $\theta + \mu$  is called a  $C_+$  characteristic; it is a left-running

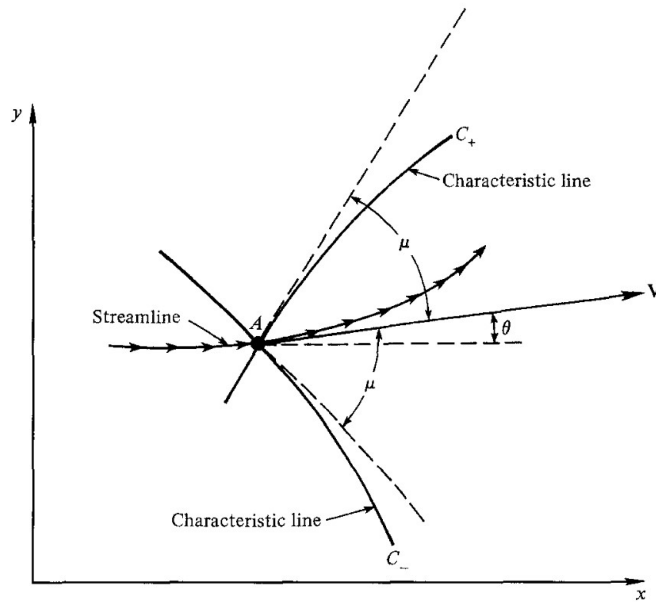


**Figure 11.8** | Illustration of left- and right-running characteristic lines.

characteristic analogous to the  $C_+$  characteristics used in Chap. 7. The characteristic in Fig. 11.8 given by the angle  $\theta - \mu$  is called a  $C_-$  characteristic; it is a right-running characteristic analogous to the  $C_-$  characteristics used in Chap. 7. Note that the characteristics are curved in general, because the flow properties (hence  $\theta$  and  $\mu$ ) change from point to point in the flow.

## 11.4 | DETERMINATION OF THE COMPATIBILITY EQUATIONS

In essence, Eq. (11.8) represents a combination of the continuity, momentum, and energy equations for two-dimensional, steady, adiabatic, irrotational flow. In Sec. 11.3, we derived the characteristic lines by setting  $D = 0$  in Eq. (11.8). In this section, we will derive the compatibility equations by setting  $N = 0$  in Eq. (11.8).

When  $N = 0$ , the numerator determinant yields

$$\begin{aligned} & \left(1 - \frac{u^2}{a^2}\right) du dy + \left(1 - \frac{v^2}{a^2}\right) dx dv = 0 \\ \text{or } & \frac{dv}{du} = \frac{-[1 - (u^2/a^2)]}{[1 - (v^2/a^2)]} \frac{dy}{dx} \end{aligned} \quad (11.15)$$

Keep in mind that  $N$  is set to zero only when  $D = 0$  in order to keep the flowfield derivatives finite, albeit of the indeterminate form 0/0. When  $D = 0$ , we are restricted to considering directions only along the characteristic lines, as explained in Sec. 11.3. Hence, when  $N = 0$ , we are held to the same restriction. Therefore, *Eq. (11.15) holds only along the characteristic lines*. Therefore, in Eq. (11.15),

$$\frac{dy}{dx} \equiv \left(\frac{dy}{dx}\right)_{\text{char}}$$

Substituting Eq. (11.10) into (11.15), we have

$$\frac{dv}{du} = -\frac{\left(1 - \frac{u^2}{a^2}\right)}{\left(1 - \frac{v^2}{a^2}\right)} \left[ \frac{-uv \pm \sqrt{\frac{u^2 + v^2}{a^2} - 1}}{\left(1 - \frac{u^2}{a^2}\right)} \right]$$

which simplifies to

$$\frac{dv}{du} = \frac{\frac{uv}{a^2} \mp \sqrt{\frac{u^2 + v^2}{a^2} - 1}}{1 - \frac{v^2}{a^2}} \quad (11.16)$$

Recall that  $u = V \cos \theta$  and  $v = V \sin \theta$ . Then, Eq. (11.16) becomes

$$\frac{d(V \sin \theta)}{d(V \cos \theta)} = \frac{M^2 \cos \theta \sin \theta \mp \sqrt{M^2 - 1}}{1 - M^2 \sin^2 \theta}$$

which, after some algebraic manipulations, reduces to

$$d\theta = \mp \sqrt{M^2 - 1} \frac{dV}{V} \quad (11.17)$$

Equation (11.17) is the *compatibility equation*, i.e., the equation that describes the variation of flow properties *along* the characteristic lines. From a comparison with Eq. (11.14), we note that

$$d\theta = -\sqrt{M^2 - 1} \frac{dV}{V} \quad (\text{applies along the } C_- \text{ characteristic}) \quad (11.18)$$

$$d\theta = \sqrt{M^2 - 1} \frac{dV}{V} \quad (\text{applies along the } C_+ \text{ characteristic}) \quad (11.19)$$

Compare Eq. (11.17) with Eq. (4.35) for Prandtl–Meyer flow. They are identical. Hence, Eq. (11.17) can be integrated to give the Prandtl–Meyer function  $v(M)$  as displayed in Eq. (4.44). Therefore, Eqs. (11.18) and (11.19) are replaced by the *algebraic compatibility equations*:

$$\theta + v(M) = \text{const} = K_- \quad (\text{along the } C_- \text{ characteristic}) \quad (11.20)$$

$$\theta - v(M) = \text{const} = K_+ \quad (\text{along the } C_+ \text{ characteristic}) \quad (11.21)$$

In Equations (11.20) and (11.21),  $K_-$  and  $K_+$  are constants along their respective characteristics, and are analogous to the Riemann invariants  $J_-$  and  $J_+$  for unsteady flow as defined in Chap. 7.

The compatibility equations (11.20) and (11.21) relate velocity magnitude and direction along the characteristic lines. For this reason, they are sometimes identified in the literature as “hodograph characteristics.” Plots of the hodograph characteristics are useful for graphical solutions or hand calculations using the method of characteristics. The reader is encouraged to read the classic texts by Ferri (Ref. 5) and Shapiro (Ref. 16) for further discussions of the hodograph approach. We shall not take a graphical approach here. Rather, Eqs. (11.20) and (11.21) are in a sufficient form for direct numerical calculations; they are the most useful form for modern computer calculations.

It is important to note that the compatibility equations (11.20) and (11.21) have no terms involving the spatial coordinates  $x$  and  $y$ . Hence, they can be solved without requiring knowledge of the geometric location of the characteristic lines. This geometrical independence of the compatibility equations is peculiar only to the present case of two-dimensional irrotational flow. For all other cases, the compatibility equations are dependent upon the spatial location, as will be discussed later.

## 11.5 | UNIT PROCESSES

In Sec. 11.2, the philosophy of the method of characteristics was given as a three-step process. Step 1—the determination of the characteristic lines—was carried out in Sec. 11.3. Step 2—the determination of the compatibility equations which hold along

the characteristics—was carried out in Sec. 11.4. Step 3—the solution of the compatibility equations point by point along the characteristics—is discussed in this section. The machinery for *applying* the method of characteristics is a series of specific computations called “unit processes,” which vary depending on whether the points at which calculations are being made are internal to the flowfield, on a solid or free boundary, or on a shock wave.

### 11.5.1 Internal Flow

If we know the flowfield conditions at two points in the flow, then we can find the conditions at a third point, as sketched in Fig. 11.9. Here, the values of  $v_1$  and  $\theta_1$  are known at point 1, and  $v_2$  and  $\theta_2$  are known at point 2. Point 3 is located by the intersection of the  $C_-$  characteristic through point 1 and the  $C_+$  characteristic through point 2. Along the  $C_-$  characteristic through point 1, Eq. (11.20) holds:

$$\theta_1 + v_1 = (K_-)_1 \quad (\text{known value along } C_-)$$

Also along the  $C_+$  characteristic through point 2, Eq. (11.21) holds:

$$\theta_2 - v_2 = (K_+)_2 \quad (\text{known value along } C_+)$$

Hence, at point 3, from Eq. (11.20),

$$\theta_3 + v_3 = (K_-)_3 = (K_-)_1 \quad (11.22)$$

and from Eq. (11.21),

$$\theta_3 - v_3 = (K_+)_3 = (K_+)_2 \quad (11.23)$$

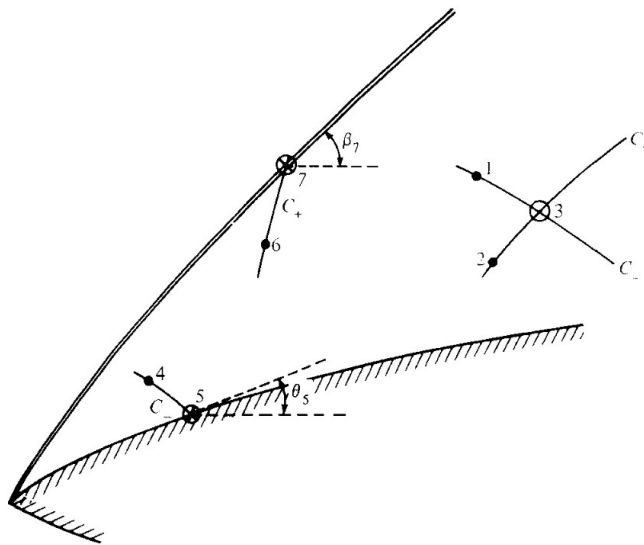


**Figure 11.9** | Unit processes for the steady-flow, two-dimensional, irrotational method of characteristics.

Solving Eqs. (11.22) and (11.23), we obtain  $\theta_3$  and  $v_3$  in terms of the known values of  $K_+$  and  $K_-$ :

$$\theta_3 = \frac{1}{2}[(K_-)_1 + (K_+)_2] \quad (11.24)$$

$$v_3 = \frac{1}{2}[(K_-)_1 - (K_+)_2] \quad (11.25)$$

Thus, the flow conditions at point 3 are now determined from the known values at points 1 and 2. Recall that  $v_3$  determines  $M_3$  through Eq. (4.44), and that  $M_3$  determines the pressure, temperature, and density through the isentropic flow relations, Eqs. (3.28), (3.30), and (3.31).

The *location* of point 3 in space is determined by the intersection of the  $C_-$  characteristic through point 1 and the  $C_+$  characteristic through point 2, as shown in Fig. 11.9. However, the  $C_-$  and  $C_+$  characteristics are generally curved lines, and all we know are their directions at points 1 and 2. How can we then locate point 3? An approximate but usually sufficiently accurate procedure is to assume the characteristics are straight-line segments between the grid points, with slopes that are average values. For example, consider Fig. 11.10. Here, the  $C_-$  characteristic through point 1 is drawn as a straight line with an average slope angle given by

$$\left[ \frac{1}{2}(\theta_1 + \theta_3) - \frac{1}{2}(\mu_1 + \mu_3) \right]$$

The  $C_+$  characteristic through point 2 is drawn as a straight line with an average slope angle given by  $\left[ \frac{1}{2}(\theta_2 + \theta_3) + \frac{1}{2}(\mu_2 + \mu_3) \right]$ . Their intersection locates point 3.

### 11.5.2 Wall Point

If we know conditions at a point in the flow near a solid wall, we can find the flow variables *at* the wall as follows. Consider point 4 in Fig. 11.9, at which the flow is known. Hence, along the  $C_-$  characteristic through point 4, the value  $K_-$  is known:

$$(K_-)_4 = \theta_4 + v_4 \quad (\text{known})$$

The  $C_-$  characteristic intersects the wall at point 5. Hence, at point 5,

$$(K_-)_4 = (K_-)_5 = \theta_5 + v_5 \quad (11.26)$$

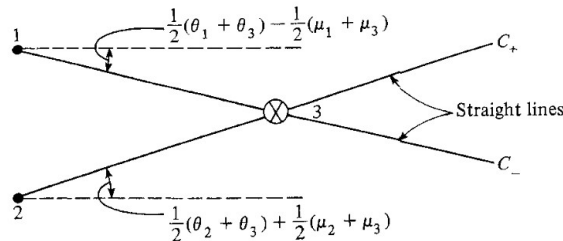


**Figure 11.10** | Approximation of characteristics by straight lines.

However, the shape of the wall is known, and since the flow must be tangent at the wall,  $\theta_5$  is known. Thus, in Eq. (11.26),  $v_5$  is the only unknown, and can be written as

$$v_5 = v_4 + \theta_4 - \theta_5$$

### 11.5.3 Shock Point

If we know conditions at a point in the flow near a shock wave, we can find the flow variables immediately behind the shock as well as the local shock angle as follows. Consider point 6 in Fig. 11.9, at which the flow is known. Hence, along the  $C_+$  characteristic through point 6, the value  $K_+$  is known:

$$(K_+)_6 = \theta_6 - v_6 \quad (\text{known})$$

The  $C_+$  characteristic intersects the shock at point 7. Hence, at point 7,

$$(K_+)_6 = (K_+)_7 = \theta_7 - v_7 \quad (11.27)$$

For a given free-stream Mach number  $M_\infty$ , find the value of the local shock angle  $\beta_7$  which yields the value of  $\theta_7 - v_7$  immediately behind the shock that agrees with the number obtained in Eq. (11.27). This is a trial-and-error process using the oblique shock relations developed in Chap. 4. Then, given  $\beta_7$  and  $M_\infty$ , all other flow properties at point 7 are known from the oblique shock relations.

### 11.5.4 Initial Data Line

The unit processes discussed in this section must *start* somewhere. In order to implement the method of characteristics, we must have a line in the locally supersonic flow along which the flowfield properties are known. Then the method of characteristics can be carried out as described here, marching downstream from the initial data line. Such a downstream-marching method is mathematically a property of hyperbolic and parabolic partial differential equations. For the calculation of an internal flow, such as a nozzle flow, the initial data line is taken at or downstream of the limiting characteristic, which is slightly downstream of the sonic line. (The concept of limiting characteristics is described in Sec. 12.3.) The properties along this initial data line must be obtained from an independent calculation, such as the time-marching method discussed in Chap. 12. An alternative for starting a nozzle calculation is simply to assume that the sonic line in the nozzle throat is straight, and to assume a centered expansion emanating from the wall of the nozzle in the throat region (see Example 11.1 in Sec. 11.7). For the calculation of an external flow, such as the flow over a sharp-nosed airfoil shape, the initial data line can be established by assuming wedge flow at the sharp leading edge, and using wedge-flow properties along a line across the flow between the body and the shock wave just a small distance downstream of the leading edge. In any event, we repeat that the method of characteristics solution for a steady supersonic flow must start from

a given initial data line, and then the calculation can be marched downstream from the line.

## 11.6 | REGIONS OF INFLUENCE AND DOMAINS OF DEPENDENCE

Our discussion on characteristic lines leads to the conclusion that in a steady supersonic flow disturbances are felt only in limited regions. This is in contrast to a subsonic flow where disturbances are felt everywhere throughout the flowfield. (This distinction was clearly made in the contrast between subsonic and supersonic linearized flow discussed in Chap. 9.) To better understand the propagation of disturbances in a steady supersonic flow, consider point  $A$  in a uniform supersonic stream, as sketched in Fig. 11.11a. Assume that two needlelike probes are introduced upstream of point  $A$ . The probes are so thin that their shock waves are essentially Mach waves. In the sketch shown, the tips of the probes at points  $B$  and  $C$  are located such that point  $A$  is outside the Mach waves. Hence, even though the probes are upstream of point  $A$ , their presence is not felt at point  $A$ . The disturbances introduced by the probes are confined within the Mach waves. On the other hand, if another probe is introduced at point  $D$  upstream of point  $A$  such that point  $A$  falls inside the Mach wave (see Fig. 11.11b), then obviously the presence of the probe is felt at point  $A$ .

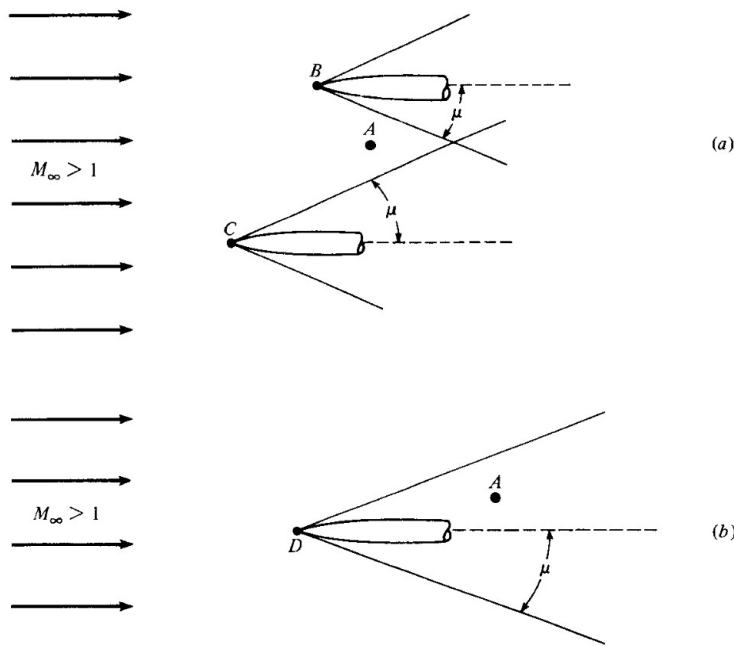


**Figure 11.11** | Weak disturbances in a supersonic flow.

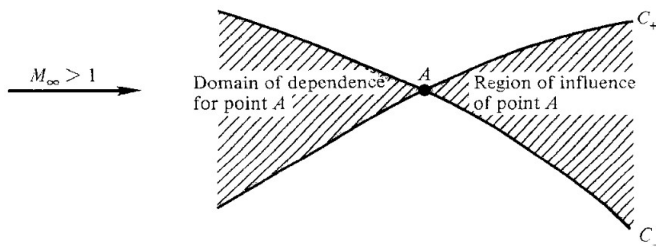


**Figure 11.12 |** Domain of dependence and region of influence.

The above simple picture leads to the definition of two zones associated with point A, as illustrated in Fig. 11.12. Consider the left- and right-running characteristics through point A. The area between the two upstream characteristics is defined as the *domain of dependence* for point A. Properties at point A “depend” on any disturbances or information in the flow within this upstream region. The area between the two downstream characteristics is defined as the *region of influence* of point A. This region is “influenced” by any action that is going on at point A. Clearly, disturbances that are generated at point A do *not* propagate upstream. This is a general and important behavior of steady supersonic flow—*disturbances do not propagate upstream*. (However, keep in mind from Chap. 7 that, in an *unsteady* supersonic flow, compression waves can propagate upstream.)

## 11.7 | SUPERSONIC NOZZLE DESIGN

In order to expand an internal steady flow through a duct from subsonic to supersonic speed, we established in Chap. 5 that the duct has to be convergent-divergent in shape, as sketched in Fig. 11.13a. Moreover, we developed relations for the local Mach number, and hence the pressure, density, and temperature, as functions of local area ratio  $A/A^*$ . However, these relations assumed quasi-one-dimensional flow, whereas, strictly speaking, the flow in Fig. 11.13a is two-dimensional. Moreover, the quasi-one-dimensional theory tells us nothing about the proper *contour* of the duct, i.e., what is the proper variation of area with respect to the flow direction  $A = A(x)$ . If the nozzle contour is not proper, shock waves may occur inside the duct.

The method of characteristics provides a technique for properly designing the contour of a supersonic nozzle for shockfree, isentropic flow, taking into account the multidimensional flow inside the duct. The purpose of this section is to illustrate such an application.

The subsonic flow in the convergent portion of the duct in Fig. 11.13a is accelerated to sonic speed in the throat region. In general, because of the multidimensionality of the converging subsonic flow, the sonic line is gently curved. However, for most applications, we can assume the sonic line to be straight, as illustrated by the straight dashed line from  $a$  to  $b$  in Fig. 11.13a. Downstream of the sonic line, the duct diverges. Let  $\theta_w$  represent the angle of the duct wall with respect to the  $x$  direction.

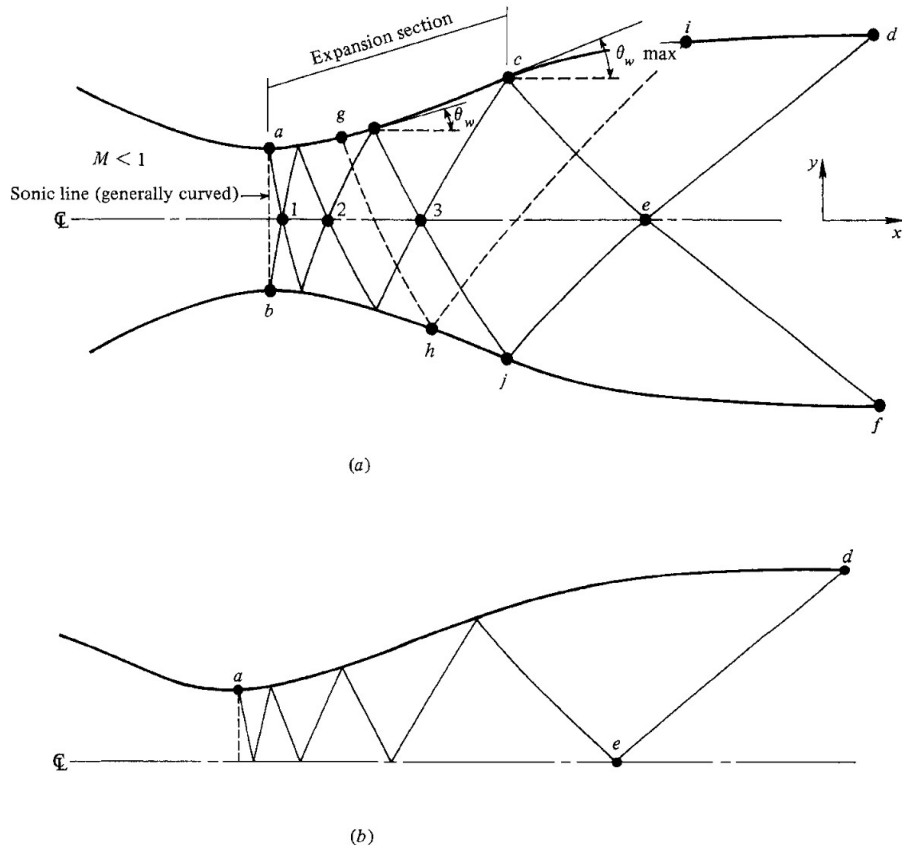


**Figure 11.13 |** Schematic of supersonic nozzle design by the method of characteristics.

The section of the nozzle where  $\theta_w$  is increasing is called the *expansion* section; here, expansion waves are generated and propagate across the flow downstream, reflecting from the opposite wall. Point *c* is an inflection point of the contour, where  $\theta_w = \theta_{w\max}$ . Downstream of point *c*,  $\theta_w$  decreases until the wall becomes parallel to the *x* direction at points *d* and *f*. The section from *c* to *d* is a “straightening” section specifically designed to cancel all the expansion waves generated by the expansion section. For example, as shown by the dashed line in Fig. 11.13a, the expansion wave generated at *g* and reflected at *h* is canceled at *i*. Also shown in Fig. 11.13a are the characteristic lines going through points *d* and *f* at the nozzle exit. These characteristics represent infinitesimal expansion waves in the nozzle, i.e., Mach waves. Tracing these two characteristics upstream, we observe multiple reflections up to the throat region. The area *acejb* is the expansion region of the nozzle, covered with both left- and right-running characteristics. Such a region with waves of both families is defined as a *nonsimple region* (analogous to the nonsimple waves described for

unsteady one-dimensional flow in Sec. 7.7). In this region, the characteristics are curved lines. In contrast, the regions *cde* and *jef* are covered by waves of only one family because the other family is cancelled at the wall. Hence, these are *simple regions*, where the characteristic lines are straight. Downstream of *def*, the flow is uniform and parallel, at the desired Mach number. Finally, due to the symmetry of the nozzle flow, the waves (characteristics) generated from the top wall act as if they are “reflected” from the centerline. This geometric ploy due to symmetry allows us to consider in our calculations only the flow above the centerline, as sketched in Fig. 11.13*b*.

Supersonic nozzles with gently curved expansion sections as sketched in Fig. 11.13*a* and *b* are characteristic of wind tunnel nozzles where high-quality, uniform flow is desired in the test section (downstream of *def*). Hence, wind tunnel nozzles are long, with a relatively slow expansion. By comparison, rocket nozzles are short in order to minimize weight. Also, in cases where rapid expansions are desirable, such as the nonequilibrium flow in modern gasdynamic lasers (see Ref. 21), the nozzle length is as short as possible. In such *minimum-length nozzles*, the expansion section in Fig. 11.13*a* is shrunk to a point, and the expansion takes place through a centered Prandtl–Meyer wave emanating from a sharp-corner throat with an angle  $\theta_{w_{\max}, M_L}$ , as sketched in Fig. 11.14*a*. The length of the supersonic nozzle, denoted as *L* in Fig. 11.14*a* is the minimum value consistent with shockfree, isentropic flow. If the contour is made shorter than *L*, shocks will develop inside the nozzle.

Assume that the nozzles sketched in Figs. 11.13*a* and 11.14*a* are designed for the same exit Mach numbers. For the nozzle in Fig. 11.13*a* with an arbitrary expansion contour *ac*, multiple reflections of the characteristics (expansion waves) occur from the wall along *ac*. A fluid element moving along a streamline is constantly accelerated while passing through these multiple reflected waves. In contrast, for the minimum-length nozzle shown in Fig. 11.14*a*, the expansion contour is replaced by a sharp corner at point *a*. There are no multiple reflections and a fluid element encounters only two systems of waves—the right-running waves emanating from point *a* and the left-running waves emanating from point *d*. As a result,  $\theta_{w_{\max}, M_L}$  in Fig. 11.14*a* must be larger than  $\theta_{w_{\max}}$  in Fig. 11.13*a*, although the exit Mach numbers are the same.

Let  $v_M$  be the Prandtl–Meyer function associated with the design exit Mach number. Hence, along the  $C_+$  characteristic *cb* in Fig. 11.14*a*,  $v = v_M = v_c = v_b$ . Now consider the  $C_-$  characteristic through points *a* and *c*. At point *c*, from Eq. (11.20),

$$\theta_c + v_c = (K_-)_c \quad (11.28)$$

However,  $\theta_c = 0$  and  $v_c = v_M$ . Hence, from Eq. (11.28),

$$(K_-)_c = v_M \quad (11.29)$$

At point *a*, along the same  $C_-$  characteristic *ac*, from Eq. (11.20),

$$\theta_{w_{\max}, M_L} + v_a = (K_-)_a \quad (11.30)$$

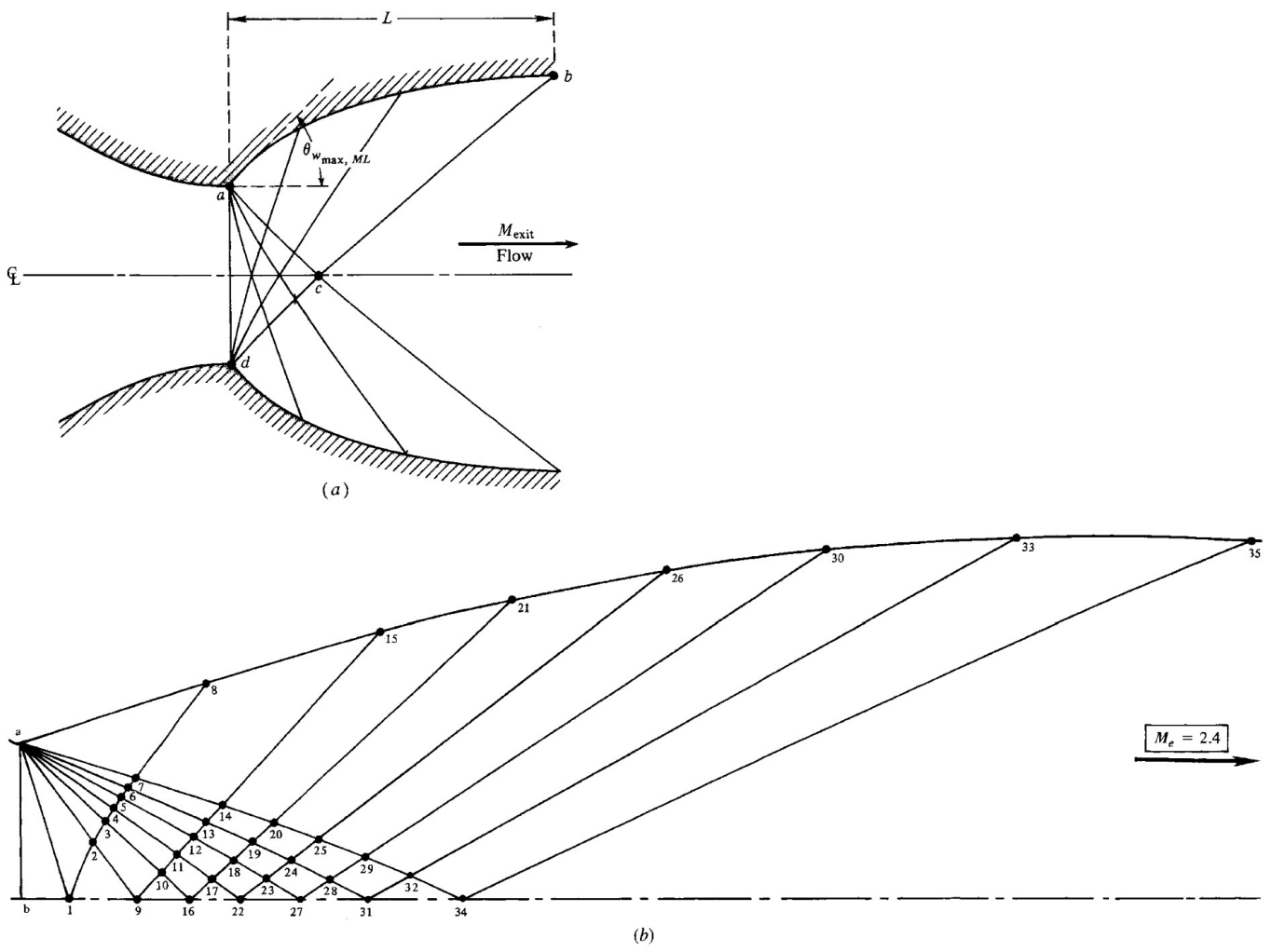


**Figure 11.14 | (a)** Schematic of minimum-length nozzle. **(b)** Graphical construction for Example 11.1.

Since the expansion at point  $a$  is a Prandtl–Meyer expansion from initially sonic conditions, we know from Sec. 4.14 that  $v_a = \theta_{w_{\max}, M_L}$ . Hence, Eq. (11.30) becomes

$$\theta_{w_{\max}, M_L} = \frac{1}{2}(K_-)_a \quad (11.31)$$

However, along the same  $C_-$  characteristic,  $(K_-)_a = (K_-)_c$ ; hence, Eq. (11.31) becomes

$$\theta_{w_{\max}, M_L} = \frac{1}{2}(K_-)_c \quad (11.32)$$

Combining Eqs. (11.29) and (11.32), we have

$$\theta_{w_{\max}, M_L} = \frac{v_M}{2} \quad (11.33)$$

Equation (11.33) demonstrates that, *for a minimum-length nozzle the expansion angle of the wall downstream of the throat is equal to one-half the Prandtl–Meyer function for the design exit Mach number*. For other nozzles such as that sketched in Fig. 11.11a, the maximum expansion angle is *less than*  $v_M/2$ .

The shape of the finite-length expansion section in Fig. 11.13a can be somewhat arbitrary (within reason). It is frequently taken to be a circular arc with a diameter larger than the nozzle throat height. However, once the shape of the expansion section is chosen, then its length and  $\theta_{w_{\max}}$  are determined by the design exit Mach number. These properties can be easily found by noting that the characteristic line from the end of the expansion section intersects the centerline at point  $c$ , where the local Mach number is the same as the design exit Mach number. Hence, to find the expansion section length and  $\theta_{w_{\max}}$ , simply keep track of the centerline Mach number (at points 1, 2, 3, etc.) as you construct your characteristics solution starting from the throat region. When the centerline Mach number equals the design exit Mach number, this is point  $c$ . Then the expansion section is terminated at point  $c$ , which fixes both its length and the value of  $\theta_{w_{\max}}$ .

### EXAMPLE 11.1

Compute and graph the contour of a two-dimensional minimum-length nozzle for the expansion of air to a design exit Mach number of 2.4.

#### ■ Solution

The results of this problem are given in Fig. 11.14b. To begin with, the sonic line at the throat,  $ab$ , is assumed to be straight. The first characteristic ( $a - 1$ ) emanating from the sharp throat is chosen as inclined only slightly from the normal sonic line. ( $\Delta\theta = 0.375^\circ$ ; hence  $\theta + v = 0.75^\circ$  and  $dy/dx = \theta - \mu = -73.725^\circ$ .) The remainder of the expansion fan is divided into six increments with  $\Delta\theta = 3^\circ$ . The total corner angle  $\theta_{w_{\max}} = v/2 = 36.75^\circ/2 = 18.375^\circ$ . The values of  $K_+$ ,  $K_-$ ,  $\theta$ , and  $v$  are tabulated in Table 11.1 for all grid points. The

Table 11.1

Point no.	$K_- =$	$K_+ =$	$\theta =$	$v =$	$M$	$\mu$	Comments
	$\theta + v$	$\theta - v$	$\frac{1}{2}(K_- + K_+)$	$\frac{1}{2}(K_- - K_+)$			
1	0.75	0	0.375 <sup>†</sup>	0.375 <sup>†</sup>	1.04	74.1	
2	6.75	0	3.375 <sup>†</sup>	3.375 <sup>†</sup>	1.19	57.2	
3	12.75	0	6.375 <sup>†</sup>	6.375 <sup>†</sup>	1.31	49.8	
4	18.75	0	9.375 <sup>†</sup>	9.375 <sup>†</sup>	1.41	45.2	
5	24.75	0	12.375 <sup>†</sup>	12.375 <sup>†</sup>	1.52	41.1	
6	30.75	0	15.375 <sup>†</sup>	15.375 <sup>†</sup>	1.62	38.1	
7	36.75	0	18.375 <sup>†</sup>	18.375 <sup>†</sup>	1.72	35.6	
8	36.75 <sup>†</sup>	0 <sup>†</sup>			1.72 <sup>†</sup>	35.6 <sup>†</sup>	Same as point 7
9	6.75 <sup>†</sup>	-6.75	0 <sup>†</sup>	6.75	1.32	49.3	
10	12.75 <sup>†</sup>	-6.75 <sup>†</sup>	3	9.75	1.43	44.4	
11	18.75 <sup>†</sup>	-6.75 <sup>†</sup>	6	12.75	1.53	40.8	
12	24.75 <sup>†</sup>	-6.75 <sup>†</sup>	9	15.75	1.63	37.8	
13	30.75 <sup>†</sup>	-6.75 <sup>†</sup>	12	18.75	1.73	35.3	
14	36.75 <sup>†</sup>	-6.75 <sup>†</sup>	15	21.75	1.84	32.9	
15	36.75 <sup>†</sup>	-6.75 <sup>†</sup>	15 <sup>†</sup>	21.75 <sup>†</sup>	1.84 <sup>†</sup>	32.9 <sup>†</sup>	Same as point 14
16	12.75 <sup>†</sup>	-12.75	0 <sup>†</sup>	12.75	1.53	40.8	
17	18.75 <sup>†</sup>	-12.75 <sup>†</sup>	3	15.75	1.63	37.8	
18	24.75 <sup>†</sup>	-12.75 <sup>†</sup>	6	18.75	1.73	35.3	
19	30.75 <sup>*</sup>	-12.75 <sup>†</sup>	9	21.75	1.84	32.9	
20	36.75 <sup>†</sup>	-12.75 <sup>†</sup>	12	24.75	1.94	31.0	
21	36.75 <sup>†</sup>	-12.75 <sup>†</sup>	12 <sup>†</sup>	24.75 <sup>†</sup>	1.94 <sup>†</sup>	31.0 <sup>†</sup>	Same as point 20
22	18.75 <sup>†</sup>	-18.75	0 <sup>†</sup>	18.75	1.73	35.3	
23	24.75 <sup>†</sup>	-18.75 <sup>†</sup>	3	21.75	1.84	32.9	
24	30.75 <sup>†</sup>	-18.75 <sup>†</sup>	6	24.75	1.94	31.0	
25	36.75 <sup>†</sup>	-18.75 <sup>†</sup>	9	27.75	2.05	29.2	
26	36.75 <sup>†</sup>	-18.75 <sup>†</sup>	9 <sup>†</sup>	27.75 <sup>†</sup>	2.05 <sup>†</sup>	29.2 <sup>†</sup>	Same as point 25
27	24.75 <sup>†</sup>	-24.75	0 <sup>†</sup>	24.75	1.94	31.0	
28	30.75 <sup>†</sup>	-24.75 <sup>†</sup>	3	27.75	2.05	29.2	
29	36.75 <sup>†</sup>	-24.75 <sup>†</sup>	6	30.75	2.16	27.6	
30	36.75 <sup>†</sup>	-24.75 <sup>†</sup>	6 <sup>†</sup>	30.75 <sup>†</sup>	2.16 <sup>†</sup>	27.6 <sup>†</sup>	Same as point 29
31	30.75 <sup>†</sup>	-30.75	0 <sup>†</sup>	30.75	2.16	27.6	
32	36.75 <sup>†</sup>	-30.75	3	33.75	2.28	26.0	
33	36.75 <sup>†</sup>	-30.75 <sup>†</sup>	3 <sup>†</sup>	33.75 <sup>†</sup>	2.28 <sup>†</sup>	26.0 <sup>†</sup>	Same as point 32
34	36.75 <sup>†</sup>	-36.75	0 <sup>†</sup>	36.75	2.4	24.6	
35	36.75 <sup>†</sup>	-36.75 <sup>†</sup>	0 <sup>†</sup>	36.75 <sup>†</sup>	2.4 <sup>†</sup>	24.6 <sup>†</sup>	Same as point 34

<sup>†</sup>Known quantities at beginning of each step.

nozzle contour is drawn by starting at the throat corner (where  $\theta_a = \theta_{w\max} = 18.375^\circ$ ), drawing a straight line with an average slope,  $\frac{1}{2}(\theta_a + \theta_8)$ , and defining point 8 on the contour as the intersection of this straight line with the left-running characteristic 7–8. Point 15 is located by the intersection of a straight line through point 8 having a slope of  $\frac{1}{2}(\theta_8 + \theta_{15})$  with the left-running characteristic 14–15. This process is repeated to generate the remainder of the contour, points 21, 26, etc.

For this example, the computed area ratio  $A_e/A^* = 2.33$ . This is within 3 percent of the value  $A_e/A^* = 2.403$  from Table A.1. This small error is induced by the graphical construction

of Fig. 11.14b, and by the fact that only seven increments are chosen for the corner expansion fan. For a more accurate calculation, finer increments should be used, resulting in a more closely spaced characteristic net throughout the nozzle.

Note that a small inconsistency is involved with the properties at point 1 in Fig. 11.14, as listed in the first line of Table 11.1. The entry in Table 11.1 for  $\theta$  at point 1 is a nonzero (but small) number, namely  $0.375^\circ$ . This is inconsistent with the physical picture in Fig. 11.14, which shows point 1 on the nozzle centerline where  $\theta = 0$ . This inconsistency is due to the necessity of *starting* the calculations with the straight characteristic line,  $a-1$ , along which the value of  $\theta$  is constant and equal to  $0.375^\circ$ . In reality, the characteristic  $a-1$  is curved because of the nonuniform flow inside the region  $a-b-1$  in Fig. 11.14, but we have no way of knowing what that nonuniform flow is for this problem. In Sec. 12.7, we will show that a finite-difference calculation in the throat region can provide such information. However, within the framework of the method of characteristics in the present section, we must live with this inconsistency. As long as the first characteristic line  $a-1$  is taken as close as possible to the assumed straight sonic line, this inconsistency will be minimized.

## 11.8 | METHOD OF CHARACTERISTICS FOR AXISYMMETRIC IRROTATIONAL FLOW

For axisymmetric irrotational flow, the philosophy of the method of characteristics is the same as discussed earlier; however, some of the details are different, principally the compatibility equations. The purpose of this section is to illustrate those differences.

Consider a cylindrical coordinate system, as sketched in Fig. 11.15. The cylindrical coordinates are  $r$ ,  $\phi$ , and  $x$ , with corresponding velocity components  $v$ ,  $w$ ,

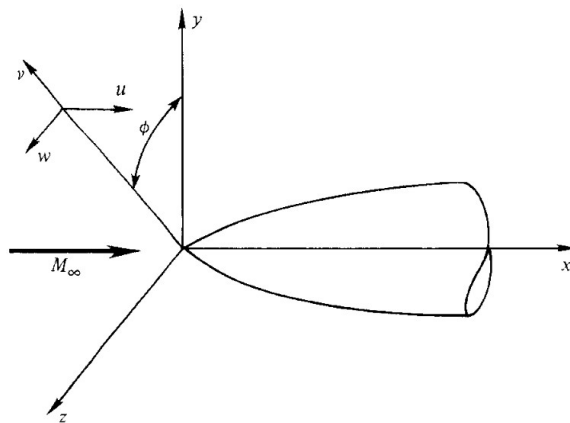


**Figure 11.15** | Superposition of rectangular and cylindrical coordinate systems for axisymmetric flow.